WCCM V
Fifth World Congress on
Computational Mechanics
July 7–12, 2002, Vienna, Austria
Eds.: H.A. Mang, F.G. Rammerstorfer,
J. Eberhardsteiner

Discontinuous Modelling of Crack Propagation in a Gradient-Enhanced Continuum

A. Simone*, G. N. Wells and L. J. Sluys

Faculty of Civil Engineering and Geosciences
Delft University of Technology, P.O. Box 5048, 2600 GA Delft, The Netherlands
e-mail: a.simone@citg.tudelft.nl

Key words: gradient damage, displacement discontinuities, fracture, enriched finite elements, partition of unity

Abstract
A numerical model for the description of the combined continuous/discontinuous failure in a regularised strain-softening continuum is proposed. The continuum is regularised through the introduction of gradient terms into the constitutive equations. At the transition to discrete failure, the problem fields are enhanced through a discontinuous interpolation based on the partition of unity concept. The discretisation procedure is described in detail and numerical examples illustrate the performance of the combined continuous/discontinuous approach.

1 Introduction

The introduction of strain softening into a continuum material description requires regularisation to preserve objective numerical results. A commonly used technique relies on the introduction of non-local interactions [1]. The performance of these so-called non-local models, in either integral or differential format, deteriorates in the final stage of failure [2]. At complete failure of a material point, which is understood as a discontinuity (*i.e.* a physical crack) in the continuum description, numerical interactions between the two physically separated parts of the body persist and cause an exchange of information between the two sides of the discontinuity. This information, in the form of locally extremely high strain values, stimulates damage growth away from the process zone, *i.e.* a spurious extension of the continuum damaged zone. This phenomenon, most evident in problems with large crack opening (*e.g.* composite failure [2]), manifests itself also in problems with small crack opening [3].
In this work, the introduction of discontinuities in a differential version of a non-local damage model is presented. Discontinuities are introduced when the material reaches a fully damaged state. By introducing a discontinuity, non-local interactions across the crack cease and the unbounded strain at the surface has no influence on the global response. Discontinuities are introduced using the partition of unity concept [4, 5], which allows discontinuities in the problem fields to cross arbitrarily through a finite element mesh [6]. It is shown that through the introduction of discontinuities in a gradient damage model, the spurious response often observed prior to complete failure is avoided. Besides this appealing numerical feature, the combined model can realistically describe macroscopic cracks.

2 Enhanced fields

In the gradient-enhanced damage continuum model proposed in [7], the problem is characterised by the displacement field $\mathbf{u}$ and by the scalar non-local equivalent strain field e. The body $\bar{\Omega}$, depicted in Fig. 1, is bounded by Γ and it is crossed by a discontinuity surface Γ_d. Displacements $\bar{\mathbf{u}}$ are prescribed on Γ_u, while tractions $\bar{\mathbf{t}}$ are prescribed on Γ_t. The internal discontinuity surface Γ_d divides the body into two sub-domains, Ω^+ and Ω^- ($\Omega = \Omega^+ \cup \Omega^-$). The boundary surface of the body $\bar{\Omega}$ consists of three mutually disjoint boundary surfaces, Γ_u, Γ_t and Γ_d ($\Gamma = \Gamma_u \cup \Gamma_t$). In the body $\bar{\Omega}$, the displacement field can be decomposed as

$$\mathbf{u}(\mathbf{x},t) = \hat{\mathbf{u}}(\mathbf{x},t) + \mathscr{H}_{\Gamma_d}(\mathbf{x})\tilde{\mathbf{u}}(\mathbf{x},t), \tag{1}$$

where $\mathscr{H}_{\Gamma_d}(\mathbf{x})$ is the Heaviside function centred at the discontinuity surface Γ_d ($\mathscr{H}_{\Gamma_d} = 1$ if $\mathbf{x} \in \Omega^+$, $\mathscr{H}_{\Gamma_d} = 0$ if $\mathbf{x} \in \Omega^-$) and $\hat{\mathbf{u}}$ and $\tilde{\mathbf{u}}$ are continuous functions on $\bar{\Omega}$. A similar decomposition holds for the non-local equivalent strain field:

$$e(\mathbf{x},t) = \hat{e}(\mathbf{x},t) + \mathscr{H}_{\Gamma_d}(\mathbf{x})\tilde{e}(\mathbf{x},t), \tag{2}$$

where $\hat{e}$ and $\tilde{e}$ are continuous functions on $\bar{\Omega}$. In the geometrically linear case, the strain field is computed as the symmetric part of the gradient of the displacement field

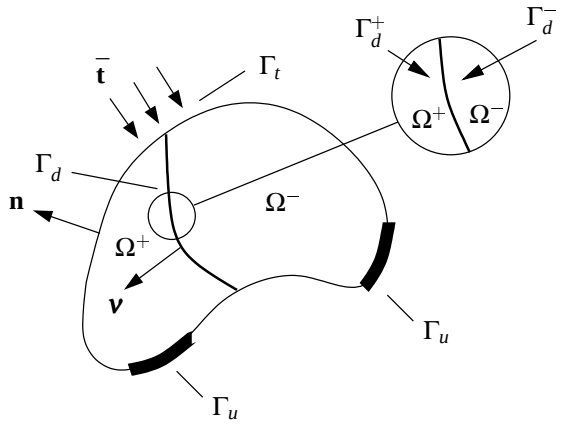

Figure 1: Body $\bar{\Omega}$ crossed by a discontinuity Γ_d.

which yields:

$$\boldsymbol{\varepsilon} = \boldsymbol{\nabla}^{\mathrm{s}}\hat{\mathbf{u}} + \mathscr{H}_{\Gamma_d}\boldsymbol{\nabla}^{\mathrm{s}}\tilde{\mathbf{u}} \quad \text{if } \mathbf{x} \notin \Gamma_d, \tag{3}$$

where $(\cdot)^{\mathrm{s}}$ refers to the symmetric part of $(\cdot)$.

3 Problem statement

The boundary value problem for the gradient-enhanced continuum is expressed by two field equations, in terms of displacements $\mathbf{u}$ and the non-local equivalent strain e, which are linked through the stress field [7]. The equilibrium equations and boundary conditions for the body $\bar{\Omega}$ without body forces can be summarised by

$$\boldsymbol{\nabla}\cdot\boldsymbol{\sigma} = \mathbf{0} \qquad \text{in } \Omega \tag{4}$$

$$\boldsymbol{\sigma}\mathbf{n} = \bar{\mathbf{t}} \qquad \text{on } \Gamma_t \tag{5}$$

where $\boldsymbol{\sigma}$ is the Cauchy stress tensor. The strong form is completed by the essential boundary condition

$$\mathbf{u} = \bar{\mathbf{u}} \qquad \text{on } \Gamma_u, \tag{6}$$

where $\bar{\mathbf{u}}$ is a prescribed displacement, and by the constitutive relation for the isotropic description of continuum damage

$$\boldsymbol{\sigma} = (1-\omega)\,\mathbf{D}{:}\boldsymbol{\varepsilon} \qquad \text{in } \Omega \tag{7}$$

in which ω is the isotropic damage parameter ($0 \leq \omega \leq 1$), function of the monotonically increasing deformation history parameter κ, $\mathbf{D}$ is the constitutive fourth order elasticity tensor and $\boldsymbol{\varepsilon}$ is the strain tensor. The evolution of the history parameter κ is governed by the Kuhn-Tucker relations:

$$\dot{\kappa} \geq 0, \qquad e-\kappa \leq 0, \qquad \dot{\kappa}\,(e-\kappa) = 0, \tag{8}$$

while an exponential softening law is used for the evolution of damage [7]:

$$\omega = 1 - \frac{\kappa_0}{\kappa}\left(1 - \alpha + \alpha e^{-\beta\left(\kappa - \kappa_0\right)}\right) \qquad \text{if } \kappa > \kappa_0, \tag{9}$$

with α and β materials parameters and κ_0 the threshold for damage initiation.
The differential format of the non-local integral averaging of the local equivalent strain ε_{eq} results in a modified Helmholtz equation for e [7]:

$$e - c\nabla^2 e = \varepsilon_{\text{eq}} \qquad \text{in } \Omega, \tag{10}$$

where c is the gradient parameter (length scale), which, together with the homogeneous natural boundary condition

$$\boldsymbol{\nabla} e \cdot \mathbf{n} = 0 \qquad \text{on } \Gamma, \tag{11}$$

completes the coupled system of equations. The equivalent strain ε_{eq} in equation (10) is expressed through the modified von Mises definition [8]:

$$\varepsilon_{\text{eq}} = \frac{k-1}{2k(1-2\nu)} I_1 + \frac{1}{2k}\sqrt{\frac{(k-1)^2}{(1-2\nu)^2} I_1^2 - \frac{12k}{(1+\nu)^2} J_2} \tag{12}$$

with I_1 and J_2 the first invariant of the strain tensor and the second invariant of the deviatoric strain tensor, respectively, k the ratio of the compressive and tensile strength and ν the Poisson's ratio.
From the decomposition of the non-local equivalent strain e and using equation (11), the boundary conditions at the discontinuity surface (cf. Fig. 1) can be written as:

$$\boldsymbol{\nabla}\hat{e} \cdot \boldsymbol{\nu} = 0 \qquad \text{on } \Gamma_d^- \tag{13}$$

$$\boldsymbol{\nabla}\left(\hat{e} + \tilde{e}\right) \cdot \boldsymbol{\nu} = 0 \qquad \text{on } \Gamma_d^+. \tag{14}$$

Since the function $\hat{e}$ is a continuous function, $\hat{e}^+ = \hat{e}^-$, where $\hat{e}^{+/-}$ indicates the value of $\hat{e}$ on $\Gamma_d^{+/-}$. Therefore,

$$\left(\boldsymbol{\nabla}\hat{e} \cdot \boldsymbol{\nu}\right) \Big|_{\Gamma_d^+} = \left(\boldsymbol{\nabla}\hat{e} \cdot \boldsymbol{\nu}\right) \Big|_{\Gamma_d^-} = 0. \tag{15}$$

From equation (15) and the above boundary conditions on Γ_d^+, it follows that $\boldsymbol{\nabla}\tilde{e} \cdot \boldsymbol{\nu} = 0$ on Γ_d^+. In summary, the boundary conditions for the non-local equivalent strain e at the discontinuity surface can be written as:

$$\boldsymbol{\nabla}\hat{e} \cdot \boldsymbol{\nu} = 0 \qquad \text{on } \Gamma_d^{+/-} \tag{16}$$

$$\boldsymbol{\nabla}\tilde{e} \cdot \boldsymbol{\nu} = 0 \qquad \text{on } \Gamma_d^+. \tag{17}$$

4 Variational formulation and discretisation

The governing system of coupled partial differential equations can be cast in a weak form. To this end, equation (4) is multiplied by a weight function $\mathbf{w}_u$, which is decomposed into $\hat{\mathbf{w}}_u$ and $\tilde{\mathbf{w}}_u$ consistent with the displacement decomposition in equation (1),

and integrated over the domain Ω:

$$\int_\Omega \left(\hat{\mathbf{w}}_u + \mathscr{H}_{\Gamma_d}\tilde{\mathbf{w}}_u\right)\cdot\left(\boldsymbol{\nabla}\cdot\boldsymbol{\sigma}\right)\,d\Omega = 0. \tag{18}$$

Following standard procedures and using the additional condition

$$\tilde{\mathbf{u}} = \mathbf{0} \qquad \text{on } \Gamma_u \tag{19}$$

for the magnitude of the displacement jump [9], the above weak equilibrium equation leads to two variational statements:

$$\int_\Omega \boldsymbol{\nabla}^{\mathrm{s}}\hat{\mathbf{w}}_u{:}\boldsymbol{\sigma}\,d\Omega = \int_{\Gamma_t}\hat{\mathbf{w}}_u\cdot\bar{\mathbf{t}}\,d\Gamma \tag{20a}$$

$$\int_{\Omega^+} \boldsymbol{\nabla}^{\mathrm{s}}\tilde{\mathbf{w}}_u{:}\boldsymbol{\sigma}\,d\Omega = \int_{\Gamma_t^+}\tilde{\mathbf{w}}_u\cdot\bar{\mathbf{t}}\,d\Gamma. \tag{20b}$$

In a similar fashion, equation (10) for the non-local equivalent strain can be recast in a variational form by multiplying it by a scalar weight function w_e (split up into $\hat{w}_e$ and $\tilde{w}_e$) and by integrating over the domain Ω:

$$\int_\Omega \left(\hat{w}_e + \mathscr{H}_{\Gamma_d}\tilde{w}_e\right)\left(\hat{e} + \mathscr{H}_{\Gamma_d}\tilde{e}\right)\,d\Omega - c\int_\Omega \left(\hat{w}_e + \mathscr{H}_{\Gamma_d}\tilde{w}_e\right)\nabla^2\left(\hat{e} + \mathscr{H}_{\Gamma_d}\tilde{e}\right)\,d\Omega = \int_\Omega \left(\hat{w}_e + \mathscr{H}_{\Gamma_d}\tilde{w}_e\right)\varepsilon_{\mathrm{eq}}\,d\Omega. \tag{21}$$

Using the product rule for the Laplacian of a discontinuous scalar field, the term $\nabla^2\left(\mathscr{H}_{\Gamma_d}\phi\right)$ in the previous equation is equal to:

$$\nabla^2\left(\mathscr{H}_{\Gamma_d}\phi\right) = \mathscr{H}_{\Gamma_d}\nabla^2\phi + \phi\boldsymbol{\nabla}\delta_{\Gamma_d}\cdot\boldsymbol{\nu} + 2\delta_{\Gamma_d}\boldsymbol{\nabla}\phi\cdot\boldsymbol{\nu}. \tag{22}$$

Substitution of the above relation into equation (21) leads to the term $\int_\Omega \phi\boldsymbol{\nabla}\delta_{\Gamma_d}\cdot\boldsymbol{\nu}\,d\Omega$ which can be expanded using the directional derivative of a function ϕ in the direction of a generic unit vector $\mathbf{v}$ ($D_{\mathbf{v}}\phi = \boldsymbol{\nabla}\phi\cdot\mathbf{v}$):

$$\int_\Omega \left(\boldsymbol{\nabla}\delta_{\Gamma_d}\cdot\mathbf{v}\right)\phi\,d\Omega = \int_\Omega D_{\mathbf{v}}\delta_{\Gamma_d}\phi\,d\Omega = -\int_{\Gamma_d} D_{\mathbf{v}}\phi\,d\Gamma = -\int_{\Gamma_d}\boldsymbol{\nabla}\phi\cdot\mathbf{v}\,d\Gamma. \tag{23}$$

Equation (23) has been derived using the following relation for the Dirac-delta function δ_{Γ_d} [10]:

$$\int_\Omega \left(\boldsymbol{\nabla}\delta_{\Gamma_d}\right)\phi\,d\Omega = -\int_{\Gamma_d}\boldsymbol{\nabla}\phi\,d\Gamma. \tag{24}$$

Using Gauss' theorem and after the application of the boundary conditions, the two variational statements generated from equation (21) can be written in the form:

$$\int_\Omega \hat{w}_e\hat{e}\,d\Omega + \int_{\Omega^+}\hat{w}_e\tilde{e}\,d\Omega + c\int_\Omega \boldsymbol{\nabla}\hat{w}_e\cdot\boldsymbol{\nabla}\hat{e}\,d\Omega + c\int_{\Omega^+}\boldsymbol{\nabla}\hat{w}_e\cdot\boldsymbol{\nabla}\tilde{e}\,d\Omega = \int_\Omega \hat{w}_e\varepsilon_{\mathrm{eq}}\,d\Omega \tag{25a}$$

$$\int_{\Omega^+} \tilde{w}_e \hat{e}\, d\Omega + \int_{\Omega^+} \tilde{w}_e \tilde{e}\, d\Omega + c\int_{\Omega^+} \boldsymbol{\nabla}\tilde{w}_e\cdot\boldsymbol{\nabla}\hat{e}\, d\Omega + c\int_{\Omega^+} \boldsymbol{\nabla}\tilde{w}_e\cdot\boldsymbol{\nabla}\tilde{e}\, d\Omega = \int_{\Omega^+} \tilde{w}_e \varepsilon_{\text{eq}}\, d\Omega. \quad (25b)$$

Finally, using a Bubnov-Galerkin approach and engineering vector notation for $\boldsymbol{\sigma}$ and $\boldsymbol{\varepsilon}$ and following standard procedures [7], the discretised boundary value problem can be written in matrix form as:

$$\begin{bmatrix} \mathbf{K}_{aa,t} & \mathbf{K}_{ab,t} & \mathbf{K}_{ap,t} & \mathbf{K}_{aq,t} \\ \mathbf{K}_{ba,t} & \mathbf{K}_{bb,t} & \mathbf{K}_{bp,t} & \mathbf{K}_{bq,t} \\ \mathbf{K}_{pa,t} & \mathbf{K}_{pb,t} & \mathbf{K}_{pp} & \mathbf{K}_{pq} \\ \mathbf{K}_{qa,t} & \mathbf{K}_{qb,t} & \mathbf{K}_{qp} & \mathbf{K}_{qq} \end{bmatrix} \begin{bmatrix} \Delta\mathbf{a} \\ \Delta\mathbf{b} \\ \Delta\mathbf{p} \\ \Delta\mathbf{q} \end{bmatrix} = \begin{bmatrix} \mathbf{f}_{\text{ext},a,t+dt} \\ \mathbf{f}_{\text{ext},b,t+dt} \\ \mathbf{0} \\ \mathbf{0} \end{bmatrix} - \begin{bmatrix} \mathbf{f}_{\text{int},a,t} \\ \mathbf{f}_{\text{int},b,t} \\ \mathbf{f}_{\text{int},p,t} \\ \mathbf{f}_{\text{int},q,t} \end{bmatrix}, \quad (26)$$

where $\Delta(\cdot)$ indicates an increment of $(\cdot)$, **a** and **b** are regular and enhanced displacement degrees of freedom, **p** and **q** are regular and enhanced non-local equivalent strain degrees of freedom and with the symmetries $\mathbf{K}_{ba} = \mathbf{K}_{ab}$, $\mathbf{K}_{bp} = \mathbf{K}_{bq} = \mathbf{K}_{aq}$, $\mathbf{K}_{qa} = \mathbf{K}_{qb} = \mathbf{K}_{pb}$, $\mathbf{K}_{qp} = \mathbf{K}_{qq} = \mathbf{K}_{pq}$ and

$$\mathbf{K}_{aa} = \int_{\Omega} \mathbf{B}_u^{\mathrm{T}} (1-\omega)\mathbf{D}\mathbf{B}_u\, d\Omega \quad (27a)$$

$$\mathbf{K}_{ab} = \int_{\Omega^+} \mathbf{B}_u^{\mathrm{T}} (1-\omega)\mathbf{D}\mathbf{B}_u\, d\Omega \quad (27b)$$

$$\mathbf{K}_{ap} = -\int_{\Omega} \mathbf{B}_u^{\mathrm{T}} \left[\frac{\partial\omega}{\partial\kappa}\right] \left[\frac{\partial\kappa}{\partial e}\right] \mathbf{D}\boldsymbol{\varepsilon}\mathbf{N}_e\, d\Omega \quad (27c)$$

$$\mathbf{K}_{aq} = -\int_{\Omega^+} \mathbf{B}_u^{\mathrm{T}} \left[\frac{\partial\omega}{\partial\kappa}\right] \left[\frac{\partial\kappa}{\partial e}\right] \mathbf{D}\boldsymbol{\varepsilon}\mathbf{N}_e\, d\Omega \quad (27d)$$

$$\mathbf{K}_{bb} = \int_{\Omega^+} \mathbf{B}_u^{\mathrm{T}} (1-\omega)\mathbf{D}\mathbf{B}_u\, d\Omega \quad (27e)$$

$$\mathbf{K}_{pa} = -\int_{\Omega} \mathbf{N}_e^{\mathrm{T}} \left[\frac{\partial\varepsilon_{\text{eq}}}{\partial\boldsymbol{\varepsilon}}\right]^{\mathrm{T}} \mathbf{B}_u\, d\Omega \quad (27f)$$

$$\mathbf{K}_{pb} = -\int_{\Omega^+} \mathbf{N}_e^{\mathrm{T}} \left[\frac{\partial\varepsilon_{\text{eq}}}{\partial\boldsymbol{\varepsilon}}\right]^{\mathrm{T}} \mathbf{B}_u\, d\Omega \quad (27g)$$

$$\mathbf{K}_{pp} = \int_{\Omega} \left(\mathbf{N}_e^{\mathrm{T}}\mathbf{N}_e + \mathbf{B}_e^{\mathrm{T}} c \mathbf{B}_e\right)\, d\Omega \quad (27h)$$

$$\mathbf{K}_{pq} = \int_{\Omega^+} \left(\mathbf{N}_e^{\mathrm{T}}\mathbf{N}_e + \mathbf{B}_e^{\mathrm{T}} c \mathbf{B}_e\right)\, d\Omega. \quad (27i)$$

As in the standard gradient damage formulation, the stiffness matrix is not symmetric. In equations (27), **N** is a matrix containing the usual finite element shape functions, **B** is a matrix containing spatial derivatives of the shape functions and κ is the maximum value of the non-local equivalent strain (see equation (8)). The terms in the RHS of the discretised boundary value problem read:

$$\mathbf{f}_{\text{int},a} = \int_{\Omega} \mathbf{B}_u^{\mathrm{T}} \boldsymbol{\sigma}\, d\Omega \quad (28a)$$

$$\mathbf{f}_{\text{int},b} = \int_{\Omega^+} \mathbf{B}_u^{\mathrm{T}} \boldsymbol{\sigma}\, d\Omega \quad (28b)$$

$$\mathbf{f}_{\text{int},p} = \int_{\Omega} \left(\mathbf{N}_e^{\mathrm{T}} \mathbf{N}_e \mathbf{p} + \mathbf{B}_e^{\mathrm{T}} c \mathbf{B}_e \mathbf{p} - \mathbf{N}_e^{\mathrm{T}} \boldsymbol{\varepsilon}_{\text{eq}} \right) \, d\Omega + \int_{\Omega^+} \left(\mathbf{N}_e^{\mathrm{T}} \mathbf{N}_e \mathbf{q} + \mathbf{B}_e^{\mathrm{T}} c \mathbf{B}_e \mathbf{q} \right) \, d\Omega \qquad (28c)$$

$$\mathbf{f}_{\text{int},q} = \int_{\Omega^+} \left(\mathbf{N}_e^{\mathrm{T}} \mathbf{N}_e \mathbf{p} + \mathbf{B}_e^{\mathrm{T}} c \mathbf{B}_e \mathbf{p} - \mathbf{N}_e^{\mathrm{T}} \boldsymbol{\varepsilon}_{\text{eq}} \right) \, d\Omega + \int_{\Omega^+} \left(\mathbf{N}_e^{\mathrm{T}} \mathbf{N}_e \mathbf{q} + \mathbf{B}_e^{\mathrm{T}} c \mathbf{B}_e \mathbf{q} \right) \, d\Omega. \qquad (28d)$$

5 Finite element implementation

The finite element implementation mainly follows the one proposed in [7] for the gradient-enhanced model. In the following, some issues pertinent to the current implementation of the discontinuous model are discussed. Other issues, such as the choice of the nodes to enhance, are discussed in [9].

Introducing a discontinuity A discontinuity is introduced when the damage at all integration points in the element ahead of a discontinuity is larger than a critical value set to $\omega_{\text{crit}} = 0.999$.

Numerical integration When dealing with integration of the element matrices only on part of an element domain, it is necessary to consider alternative integration rules. When an element is intersected by a discontinuity, the two resulting sub-domains are triangulated and each sub-domain is mapped to a parent unit triangle over which a three-point symmetric quadrature rule, with interior points within the triangular sub-domain, is considered [9].

6 Failure analysis of a concrete beam in four-point bending

To illustrate the combined continuous/discontinuous approach, a four-point bending test of a concrete beam with different notch sizes d is analysed (Fig. 2). To enable comparison with the experiments [11], the vertical displacement of a point placed at the bottom of the beam and with an offset of 7.5 mm from the centreline of the beam is used for the measurement of the deflection v. The following material parameters [3], 'fitted' for the continuum problem, are adopted for the simulation: Young's modulus $E = 40000\ MPa$; Poisson's ratio $\nu = 0.2$; exponential damage evolution law (equation (9)) with damage threshold $\kappa_0 = 0.000075$, damage law parameters $\alpha = 0.92$ and $\beta = 300$; modified von Mises definition of the local equivalent strain (equation (12)) with $k = 10$; gradient parameter $c = 4\ mm^2$. The simulation is performed under plane stress conditions. The load is applied via an imposed displacement. Quadrilateral elements with quadratic interpolation for the displacement and linear interpolation for the non-local equivalent strain have been used. A 2×2 Gauss quadrature rule is used in the continuum for elements not crossed by a discontinuity. The notch is simulated as a traction-free discontinuity [9] and the direction of the discontinuity is prescribed to be vertical. The analyses for the 10 mm deep notch beam are reported in Fig. 3a for different mesh sizes. In the process zone, the coarse, medium and fine mesh element sizes are, respectively, 10 mm, 5 mm and 2.5 mm. Due to the small difference in the response between the medium and the fine discretisation (Fig. 3a), the former, with a 10 mm deep notch, has been used for the results depicted in Fig. 4 and Fig. 5. From the analysis of the results it is evident how the introduction of a discontinuity during

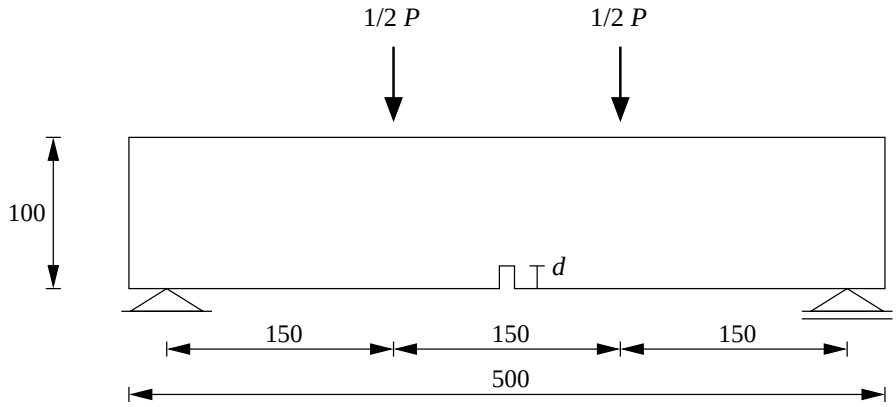

Figure 2: Four-point bending test (thickness 50 mm; dimensions in mm).

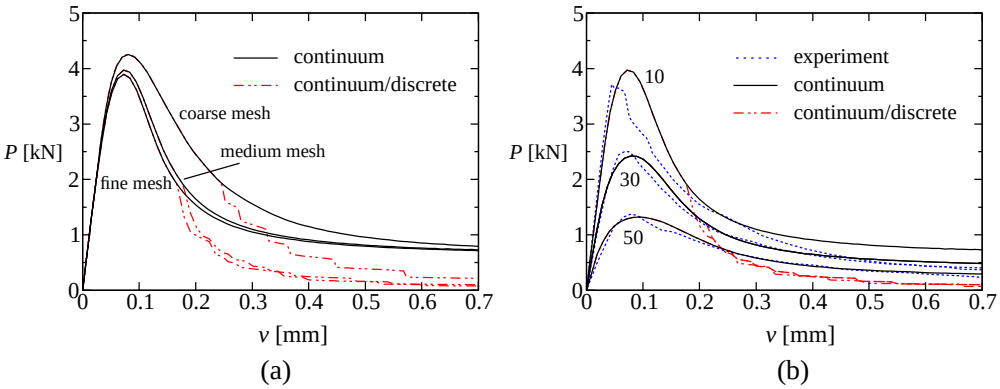

Figure 3: Load-deflection curves for simulations with (a) different meshes (10 mm deep notch) and (b) different notch size d (medium mesh) and experimental results [11].

the computation influences the global and local behaviour. In particular, Fig. 4 shows how the activity of the non-local equivalent strain is mobilised only around the discontinuity tip for the continuum/discrete model. This translates in the more realistic damage profiles depicted in Fig. 5. However, the use of an exponential softening relationship with a high residual stress at the moment of the enhancement (around 10 % of the tensile strength) causes the marked drops in Fig. 3a and makes the comparison with experiment difficult (Fig. 3b). The use of different stress-strain relationships with lower residual stress values produced an unsatisfactory comparison in the post-peak response. Introduction of displacement discontinuities requires a re-assessment of the material parameters of the continuum model which govern the post-peak response.

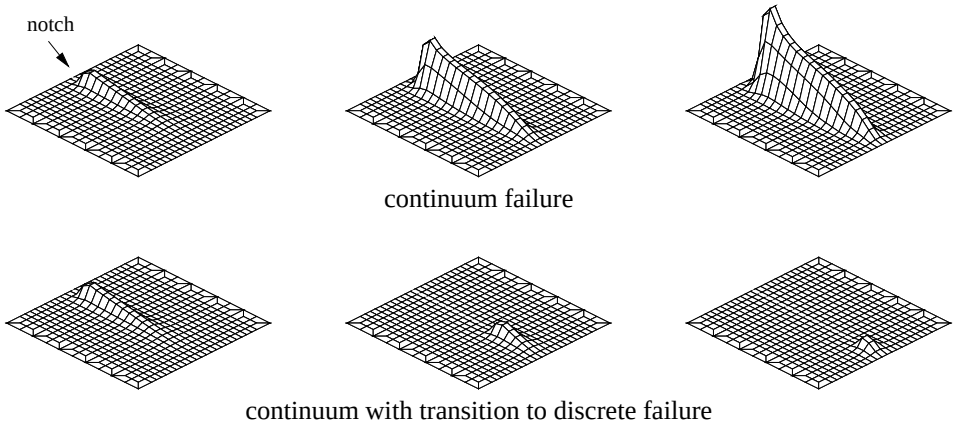

Figure 4: Four-point bending test: non-local equivalent strain evolution (medium mesh / 10 mm deep notch beam).

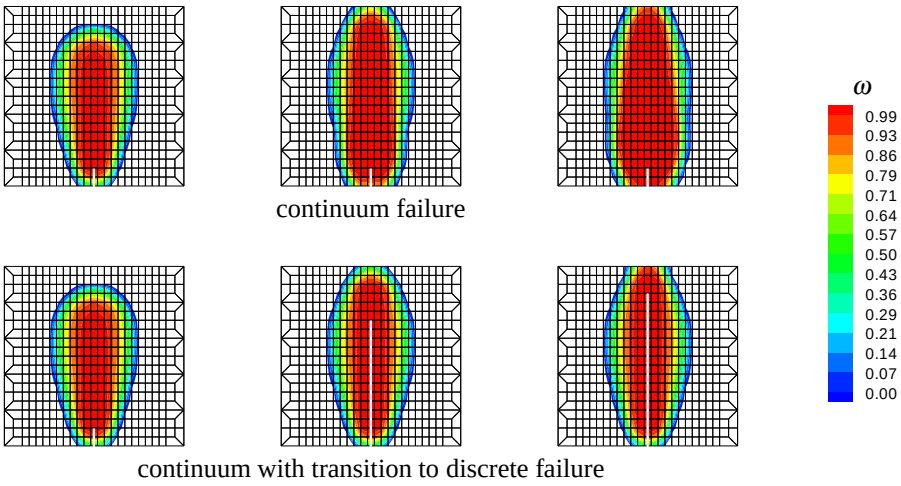

Figure 5: Four-point bending test: damage evolution (the discontinuity is represented by the white thick line; medium mesh / 10 mm deep notch beam).

7 Conclusions

A discontinuous gradient-enhanced damage model for fracture has been presented. An implicit gradient-enhanced damage model is enriched with discontinuous interpolations of the problem fields through the partition of unity concept. The discretisation procedure for the enriched model has been completely described. By introducing a discontinuity at a fully damaged material point, macroscopic cracks can be realistically described. As a discontinuity propagates, the activity of the non-local equivalent strain is mobilised at the discontinuity tip and ceases behind it. Spurious growth of damage can thus be prevented since the non-local interaction between the two sides of the discontinuity is avoided.

Acknowledgements

Financial support to the first author through the BEO programme (special fund from TU Delft for excellent research) is gratefully acknowledged.

References

[1] G. Pijaudier-Cabot, Z. Bažant, *Nonlocal damage theory,* ASCE Journal of Engineering Mechanics, 113, (1987), 1512–1533.

[2] M. G. D. Geers, R. de Borst, W. A. M. Brekelmans, R. H. J. Peerlings, *Strain-based transient-gradient damage model for failure analyses,* Computer Methods in Applied Mechanics and Engineering, 160, (1998), 133–153.

[3] J. Pamin, R. de Borst, *Gradient-enhanced damage and plasticity models for plain and reinforced concrete*, in W. Wunderlich, ed., *Proceedings of the European Conference on Computational Mechanics ECCM'99*, Technical University of Munich, Munich (1999), pp. 482–483, paper no. 636.

[4] C. A. M. Duarte, J. T. Oden, *H-p clouds – an h-p meshless method*, Numerical Methods for Partial Differential Equations, 12(6), (1996), 673–705.

[5] J. M. Melenk, I. Babuška, *The partition of unity finite element method: Basic theory and applications,* Computer Methods in Applied Mechanics and Engineering, 139(1–4), (1996), 289–314.

[6] N. Moës, J. Dolbow, T. Belytschko, *A finite element method for crack growth without remeshing*, International Journal for Numerical Methods in Engineering, 46(1), (1999), 131–150.

[7] R. H. J. Peerlings, R. de Borst, W. A. M. Brekelmans, J. H. P. de Vree, *Gradient-enhanced damage for quasi-brittle materials,* International Journal for Numerical Methods in Engineering, 39, (1996), 3391–3403.

[8] J. H. P. de Vree, W. A. M. Brekelmans, M. A. J. van Gils, *Comparison of nonlocal approaches in continuum damage mechanics,* Computers and Structures, 55, (1995), 581–588.

[9] G. N. Wells, L. J. Sluys, *A new method for modelling cohesive cracks using finite elements,* International Journal for Numerical Methods in Engineering, 50(12), (2001), 2667–2682.

[10] I. Stakgold, *Green's Functions and Boundary Value Problems*, John Wiley and Sons, New York (1979).

[11] D. A. Hordijk, *Local approach to fatigue of concrete,* Ph.D. thesis, Delft University of Technology (1991).